Journal of Archaeological Science 137 (2022) 105507

Contents lists available at ScienceDirect

Journal of Archaeological Science

journal homepage: www.elsevier.com/locate/jas

Not a bathtub: A consideration of sea-level physics for archaeological models of human migration

Marisa Borreggine [a,*], Evelyn Powell [a], Tamara Pico [b,c], Jerry X. Mitrovica [a], Richard Meadow [d], Christian Tryon [d,e,f]

[a] Harvard University, Department of Earth and Planetary Sciences, 20 Oxford Street, Cambridge, MA, 02138, USA
[b] California Institute of Technology, Division of Geological and Planetary Sciences, 1200 E California Boulevard, Pasadena, CA, 91125, USA
[c] University of California, Santa Cruz, Department of Earth and Planetary Sciences, 1156 High Street, Santa Cruz, CA, 95064, USA
[d] Harvard University, Department of Anthropology, 11 Divinity Avenue, Cambridge, MA, 02138, USA
[e] University of Connecticut, Department of Anthropology, 354 Mansfield Road, Storrs, CT, 06269, USA
[f] Human Origins Program, National Museum of Natural History, Smithsonian Institution, 10th and Constitution Ave., NW, Washington, DC, 20560, USA

ARTICLE INFO

Keywords:
Migration
Numerical modeling
Sea-level change
Glacial isostatic adjustment
Paleogeography
Deglacial

ABSTRACT

Accurately reconstructing past sea level is key to simulating potential migration pathways of ancient hominins, including early *Homo sapiens*. Models of ancient human migration events commonly construct estimates of paleoenvironments using the "bathtub" model, in which sea level is assumed to rise and fall according to a "eustatic" (global average) value over time. However, large uncertainties exist on past ice sheet sizes and shapes, particularly prior to the Last Glacial Maximum (LGM), ~26,000 years ago. Moreover, regional sea level varies significantly due to the effects of glacial isostatic adjustment (GIA). That process includes Earth's gravitational, deformational, and rotational response to changing surface (ice plus ocean) loads across the ice age. Here, we offer an updated account of the physics of GIA-induced sea-level change and consider the impacts of these effects, together with a newly published ice sheet history, on sea-level changes across the last glacial cycle. As illustrations, we highlight the significance of these issues for studies of ancient human migration from Sunda to Sahul and for the timing of the final, post-LGM flooding of the Strait of Dover. These examples demonstrate the importance of incorporating updated ice sheet histories and accurate sea-level physics into archaeological research.

1. Introduction

Understanding sea-level change is critical for studies of past human-landscape interaction. Sea level is not static. As continental ice sheets waxed and waned according to Earth's past climatic conditions, water correspondingly transferred out of and into the ocean basins (Peltier, 1982; Nakada and Lambeck, 1989; Mitrovica and Milne, 2002; Milne and Mitrovica, 2008; Lambeck et al., 2014). Global mean sea-level (GMSL), sometimes called eustatic change, an almost-direct measure of past ice volume, is estimated using geological markers of sea level (e.g., uplifted beach terraces) and proxy data – notably oxygen isotope stratigraphy from foraminifera shells in deep-sea sedimentary cores (e.g., Waelbroeck et al., 2002; Lisiecki and Raymo, 2005). Because changes in sea level shape topography and influence regional oceanographic conditions, sea level is a major factor controlling the dispersal of humans and other animal and plant taxa. For example, the feasibility of specific migration routes is affected by changing oceanic currents, wind patterns (Kuijjer, 2020), and the distance between shorelines (including the formation of land bridges; Robles, 2013). Knowing these routes precisely can illuminate both the regional paleoenvironment and potential human impacts on flora and fauna.

Archaeological migration studies generally employ a "bathtub" model that uniformly lowers and raises sea level globally to reconstruct ancient shoreline positions (Birdsell, 1977; Hoffecker et al., 2016; Kealy et al., 2018). These traditional reconstructions of past sea level are subject to two significant sources of error that could bias inferences of most-likely migration pathways. First, the conversion between ice volume proxies such as oxygen isotope anomalies in ocean sedimentary cores and GMSL is uncertain (Waelbroeck et al., 2002). We discuss recent improvements to estimates of past ice sheet volume and geometry

* Corresponding author.
E-mail address: mborreggine@g.harvard.edu (M. Borreggine).

https://doi.org/10.1016/j.jas.2021.105507
Received 9 April 2021; Received in revised form 19 October 2021; Accepted 19 October 2021
Available online 11 November 2021

in Section 2. Second, regional sea-level changes can depart significantly from GMSL adopted in a "bathtub" model (Milne and Mitrovica, 2008). Surface (ice and ocean) mass loading leads to deformation of Earth's surface and perturbations to both the gravitational field and rotation axis. This suite of effects, termed glacial isostatic adjustment (GIA), impacts local sea level, even in areas of the ocean far removed from changing ice sheets (e.g., Milne and Mitrovica, 2008).

A number of archaeological studies of human settlement and migration have benefitted from inclusion of more accurate sea-level physics in reconstructing paleo-landscapes. In pioneering work, Lambeck and colleagues have demonstrated the importance of applying GIA models of ice age sea-level change in archaeology studies, with case studies including human migrations out of Africa via the Red Sea (Lambeck et al., 2011), across the Aegean in the Upper Paleolithic and Neolithic (Lambeck, 1996a), and in the settlements of lower Mesopotamia during the Holocene (Lambeck, 1996b). Clark et al. (2014) used state-of-the-art sea-level modeling to reconstruct coastal paleogeography of the California-Oregon-Washington and Bering Sea continental shelves and their connection to the initial peopling of the Americas. Spada and Galassi (2017) investigated the impact of GIA on studies of *aquaterra* (i.e., land that is flooded and exposed in step with interglacial and glacial periods) in Doggerland and Beringia, regions relevant to early human migration and landscape use (see also Dobson et al., 2020).

The present study has two primary goals. The first is to highlight new constraints on ice history and GMSL across the last glacial cycle, a window of time that encompasses seminal episodes of ancient human migration across oceans. The second is to provide the archaeological community with a comprehensive, generalized description of sea-level physics. To illustrate these issues, we consider shoreline reconstructions across two separate time periods. The first is relevant to the initial peopling of Australia, wherein *Homo sapiens* migrated through Sunda (a region that includes modern-day Indonesia) and into Sahul (a region that includes modern-day Australia) ca. 65,000–45,000 years ago. Due to its shallow bathymetry, the central Indo-Pacific region is susceptible to drastic changes in land availability caused by minor variations in reconstructed sea level. This example will particularly highlight the importance of recent revisions to GMSL history across the last glacial phase of the ice age. Second, we consider estimates of the timing of the post-LGM sea-level rise across the Strait of Dover based on GIA modeling and under the "bathtub" assumption. Since the GMSL curve for the LGM to Late Holocene is well established, this example highlights the impact of sea level physics beyond the bathtub.

2. Improvements to GMSL and ice sheet reconstructions

Two GMSL curves commonly used to reconstruct paleotopography in the archaeological community are based on the study of Lambeck and Chappell (2001) (hereafter LC01) and the ICE-5G ice history (Peltier and Fairbanks, 2006). Fig. 1 shows GMSL curves extending from the Last Interglacial (LIG, ~120 ka) through the Last Glacial Maximum (LGM, ~26 ka) to present day. The pre-LGM component of the LC01 curve (purple line) is based on tectonically uplifted and exposed reefs from the Huon Peninsula on New Guinea (Lambeck and Chappell, 2001). In contrast, the pre-LGM history of the ICE-5G model (black line) is constrained, in large part, by a GMSL history inferred by Martinson et al. (1987) from oxygen isotope records in the South Indian Ocean (Peltier and Fairbanks, 2006).

Although the time period from the termination of the LIG to the LGM is characterized by data sparsity, new constraints have been incorporated into the latest ice reconstructions for this period. Peak GMSL at 46 ka has been constrained by sea-level changes recorded in sedimentary cores from China's Yellow River Delta (Pico et al., 2016) and sea-level markers (marine lithofacies and terrestrial facies in sediment cores and outcrops) along the East Coast of the U.S.A. (Pico et al., 2017). Furthermore, Creveling et al. (2017) constrained peak GMSL at ~100 ka and ~80 ka by comparing sea-level highstand records (marine terraces,

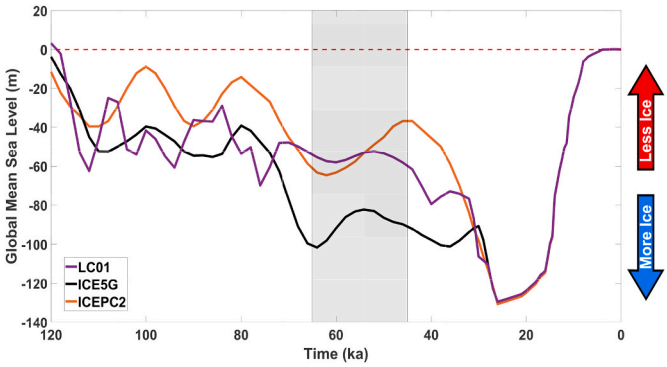

Fig. 1. GMSL and ice history reconstructions. Global mean sea-level change relative to present day for three different models: LC01 (purple line), ICE-5G (black line), and ICEPC2 (orange line) (note that ICEPC2 and ICE-5G have identical GMSL variation post-LGM). The dashed red line represents present-day sea level. The gray shaded region denotes the time period of interest for the case study discussed in Section 5.1. (For interpretation of the references to color in this figure legend, the reader is referred to the Web version of this article.)

dated corals, and oxygen isotope records) to GIA modeling of sea-level changes. These inferences have been incorporated in the ice model ICEPC2 (Fig. 1, orange line), which revises the ICE-5G reconstruction of ice volume and geometry prior to LGM (Pico et al., 2017). (The two models are identical in the post-LGM period, and thus the orange and black lines overlap from ~25 ka to present.) Note that the shallower ocean depths estimated by the GMSL curve for ICEPC2 imply a significant (approximately three-fold) increase in total ice volume from 46 ka to the LGM. This increase is driven by a late-stage glaciation of the eastern sector of the Laurentide Ice Sheet over Canada, which is consistent with new sedimentological and biological evidence from the region (Dalton et al., 2016, 2019; Pico et al., 2018).

The ICE-5G reconstruction of GMSL differs from the LC01 and ICEPC2 inferences by ~50 m at 64 ka. In northern Australia and across Sunda, this departure translates to a difference of landmass exposure of ~1,000,000 km^2, roughly the size of modern-day Egypt, resulting in a substantially different landscape for early occupation and dispersal. At 46 ka, the difference between ICE-5G and LC01 GMSL is ~32 m; between ICE-5G and ICEPC2 the discrepancy is ~53 m. In contrast to this level of disagreement, GMSL is well constrained in the post-LGM period through sediment and coral records with associated radiocarbon or uranium-series dating (among other proxies; Lambeck et al., 2014). Although there is general consensus in regard to the GMSL curve for this time period, elements of the ice geometries continue to be revised. In particular, which ice sheets contributed to the global sea-level rise remains debated (e.g., Lambeck et al., 2014; Liu et al., 2016; Simms et al., 2019; Lin et al., 2021).

3. Sea-level physics

Sea level is formally defined as the vertical distance between the sea surface and the solid surface (e.g., the ocean floor), and changes in sea level can arise from perturbations to the elevation of either boundary. (We note that, with this definition of sea level, changes to topography are the negative of changes to sea level; Farrell and Clark, 1976; Kendall et al., 2005). The sea surface is defined here as a gravitational equipotential (we neglect ocean tides and the dynamic effects of wind-driven ocean circulation). In the "bathtub" model, sea-level changes are assumed to be uniform and reflect the lowering/rising of the sea surface in response to continental and grounded marine ice sheets growing/melting. Fig. 2 provides a schematic summary of the physics of ice age sea-level change neglected by the "bathtub" model. We discuss each of these effects in detail below and return to them, as applicable, in our

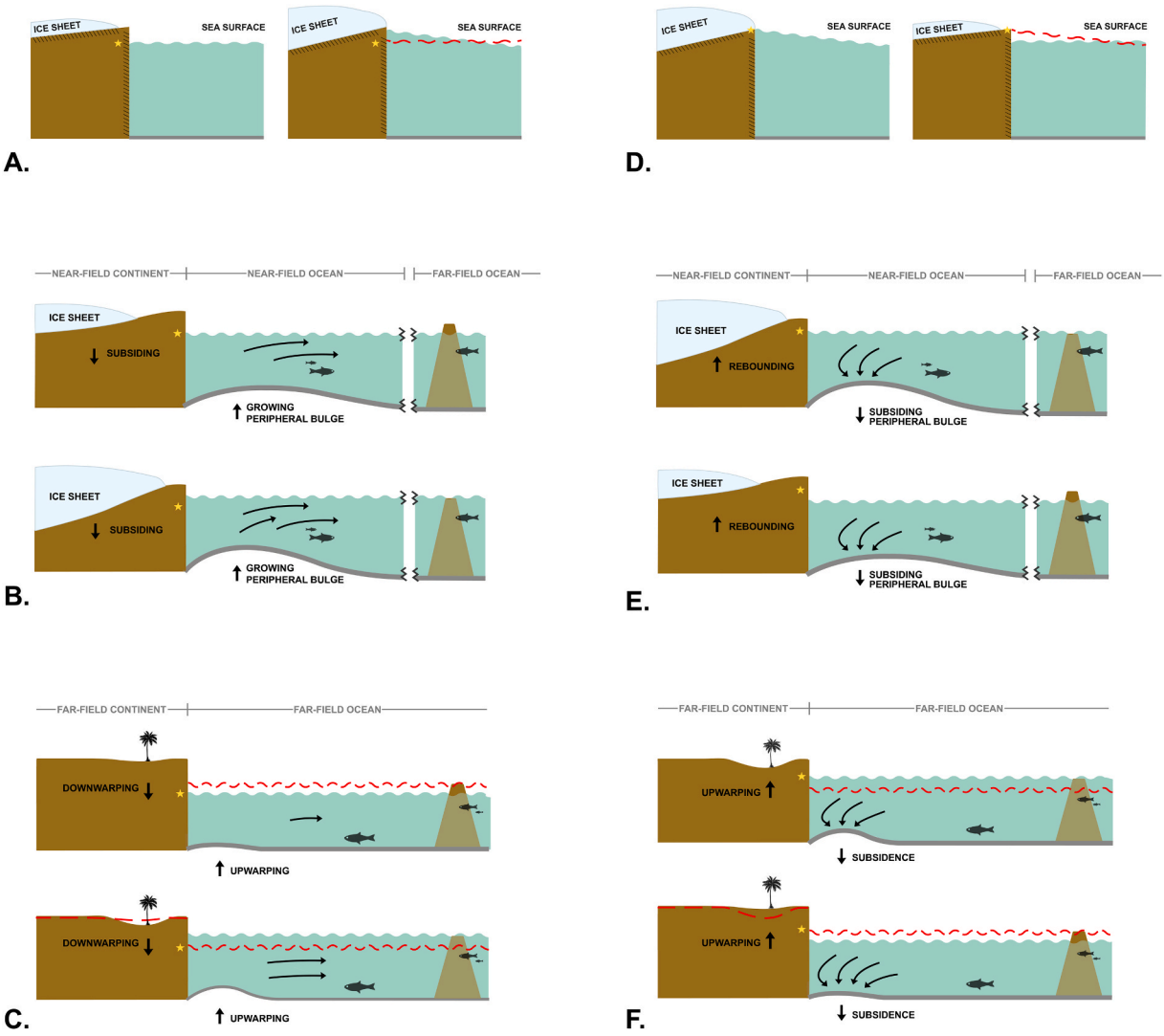

Fig. 2. The physics of ice age sea-level change. GIA processes active during (A–C) glaciations and (D–F) deglaciation and interglacials (see Section 3). The top row shows self-gravitation during periods of active ice mass change; middle row illustrates crustal deformation processes in the near-field of ice cover (at left) and the contribution of peripheral bulge dynamics to ocean syphoning (at right); bottom row shows crustal deformation (continental levering) along far-field continental shorelines (at left) and the contribution of this process to ocean syphoning (at right).

case studies (Section 5).

One process not considered by the "bathtub" model is "load self-gravitation," which perturbs the sea surface and leads to geographically variable sea-level change (Farrell and Clark, 1976). This process, illustrated in Fig. 2A and D, occurs because ice sheets and glaciers exert a gravitational pull on the surrounding ocean. As an ice sheet grows, that pull increases and water migrates toward the ice sheet, resulting in a sea-level rise that extends approximately two thousand kilometers from the zone of growth (Mitrovica et al., 2018) – roughly the distance between southern Japan and the northern Philippines (Fig. 2A). At greater distances, sea level generally falls by progressively larger amounts. A melting ice sheet will have the opposite effect on sea level. The decreased gravitational pull causes the surrounding ocean to migrate away from the ice sheet resulting in a sea-level fall in the "near-field" and sea-level rise in the "far-field" (Fig. 2D). This gravitationally-driven redistribution of water mass is essentially instantaneous, and its magnitude is significant. For example, if an ice sheet melts enough to raise GMSL by 1 m, the sea-level fall at the edge of the ice sheet will have an amplitude on the order of 10 m, and the peak sea-level rise at distance from the melt zone can reach 40% higher (up to 1.4 m in this example) than the GMSL rise (Mitrovica et al., 2018).

The solid Earth (crust and mantle) responds to any type of forcing (e.g., changes in surface loading, such as a growing or melting ice sheet, or changes in a stress field, such as an earthquake) in a manner that is dependent on the time scale of that forcing (Peltier, 1982). For example, on fast timescales (seconds to hours) a rapid rupture of the Earth's crust instantaneously produces earthquakes and seismic waves that largely propagate elastically through the Earth's mantle (Dahlen and Tromp, 1998). Continental drift, on the other hand, is driven by slow viscous flow within the Earth's mantle (commonly described as a "viscous solid") that has a time scale of tens of millions of years (Turcotte and Schubert, 2014). Ice age sea-level changes represent a complicated intermediate case. Across an ice age, variations in ice volume and geometry generally occur on time scales of thousands of years or longer, and the associated ice-plus-ocean load changes drive perturbations to the gravity field and deformation of the solid Earth that include *both* a rapid (effectively instantaneous) elastic component and a delayed viscous signal (Peltier, 1982). This viscoelastic response is reflected in sea-level changes, as we describe below. An important point to note is that sea-level changes due to the ice age persist to the present day even though ice volumes remained relatively constant over the past 6 millennia, i.e., the present interglacial (Mitrovica and Milne, 2002).

These ongoing changes reflect the delayed viscous response to ice age loading.

Recalling our definition of sea level, uplift of the solid surface (rise in topography) will lead to a local sea-level fall, while subsidence (fall in topography) will lead to a local sea-level rise. Similarly, a drop of the sea surface will produce a local sea-level fall, while a rise of this surface leads to a sea-level rise. In the following, as in the figures describing self-gravitation, we will consider the details of the various processes both within the glaciation phase that begins a glacial cycle (Fig. 2B and C) and during the deglaciation phase that ends it (Fig. 2E and F). However, the physics we describe for the deglaciation phase continue beyond the end of the deglaciation into the subsequent interglacial because of the delayed viscous effects described above. Thus, the right column of Fig. 2 captures sea-level physics occurring during both the deglaciation phase and in the subsequent interglacial.

The sections of Fig. 2B and E labeled near-field focus on processes relatively close to the ice sheets (or their former location) that are dominated by deformational effects. As an ice sheet grows, the excess mass loads and depresses the underlying crust, causing local sea level to rise, and, in addition, mantle material within the Earth's interior is pushed outward from the area of loading, creating what is termed a "peripheral bulge" (Fig. 2B; Mitrovica and Milne, 2002). These peripheral bulges surround all regions with continental ice sheets during the LGM, and their growth leads to a local sea-level fall. When an ice sheet melts, the reverse occurs. The area beneath the ice load begins to slowly rebound, initiating a period of local sea-level fall, while the peripheral bulge subsides, and local sea-level rises, as mantle material returns from these peripheral regions toward the zone of rebound (Fig. 2E).

The uplift/subsidence of the peripheral bulges in the ocean leads to a process called "ocean syphoning," where water moves toward/away from the far-field of the ice cover (i.e., areas of the Earth far from glaciated regions; see labels on Fig. 2; Mitrovica and Peltier, 1991; Mitrovica and Milne, 2002). Fig. 2B illustrates the process during a period of ice sheet growth. In this case, the uplift of the bulge pushes water outward toward the far-field, which experiences a sea-level rise. In contrast, during the deglaciation phase and subsequent interglacial, water migrates toward the ice sheets to fill the space vacated by the subsiding peripheral bulge, leading to a local sea-level fall in the far-field (Fig. 2E). Note that in the near-field region of the peripheral bulge, local sea-level changes are due largely to local crustal deformation, whereas in the far-field the local sea-level change is dominated by changes in the height of the sea surface.

As ice sheets grow or melt, water moves from or into the global ocean and this redistribution of ocean mass itself acts as a changing load on the oceanic crust. Ocean loading has the greatest impact near shorelines, where material in the Earth's mantle moves most easily between the region under the continent to under the sea floor, or vice versa (Fig. 2C and F). During the glaciation phase, water is taken up by ice sheets and unloads the far-field ocean. This mass exchange leads to uplift of the oceanic side of the shoreline and subsidence on the continental side, effectively tilting the crust in a process called "continental levering" (Fig. 2C; Nakada and Lambeck, 1989; Mitrovica and Milne, 2002). This contributes a sea-level fall on the ocean side and sea-level rise on the continent side of the shoreline. In addition, the net flow of water away from these regions of uplifting oceanic crust acts to raise sea level in the open ocean (Fig. 2C, far right). During the deglaciation phase and subsequent interglacial, the reverse occurs (Fig. 2F). The increased ocean load in this case leads to subsidence of the oceanic crust near the shoreline, and thus to a local sea-level rise (Fig. 2F, at left), uplift of the crust and sea-level fall on the continent side (far left), and sea-level fall in the open ocean (far right).

The impact of continental levering on far-field sea level (far right, Fig. 2C and F) is considered to be a second contribution to the ocean syphoning mechanism since it reinforces the far-field impacts of peripheral bulge dynamics illustrated in Fig. 2B and E (Mitrovica and Milne, 2002). That is, both processes migrate water toward, and raise sea level in, the far-field open ocean during the glaciation phase, and migrate water away from, and lower sea level in, the far-field open ocean during deglaciation and the subsequent interglacial.

There is a final effect on sea level related to Earth rotation. Mass exchange between ice sheets and oceans, and the solid Earth deformation associated with this exchange, will reorient the rotation axis of the Earth and this reorientation will also drive a sea-level signal. In the case studies explored below, this effect is relatively small (typically of a magnitude of a few meters), and while it is included in the sea-level theory we adopt (Kendall et al., 2005), we will not discuss it further. We also do not consider in detail the effects of vertical land motion due to tectonic activity, erosion, and sedimentation on sea-level change. Although they may be important considerations at specific geographic sites (Pirazolli, 2005; Pico et al., 2016; Pico, 2020), they are outside the scope of this more general review.

We can use the example of the present interglacial to provide a sense of the magnitude of sea-level changes associated with the various processes described above. During the last few thousand years, post-glacial rebound near the center of areas with significant glaciation at LGM (Fig. 2E, left), e.g., North America's Hudson Bay and northern Europe's Gulf of Bothnia, have experienced a sea-level fall in the order of 1 cm/yr (Mitrovica and Milne, 2002), leading to the raised ancient beach terraces that are pervasive in these regions (e.g., Pendea et al., 2010) and the emergence of previously submerged islands (Tsuji et al., 2016). The peripheral subsidence of the crust encircling these areas of LGM ice cover during the present interglacial (which includes both coasts of the continental United States) has driven a sea-level rise of up to 3–5 mm/yr (Mitrovica and Milne, 2002), which has led to an inland encroachment of the ocean and contributes to the flooding of archaeological sites reflecting near-shore activities of early humans (e.g., Fedje and Josenhans, 2000). Finally, ocean syphoning and continental levering have combined during the present interglacial to contribute a net sea-level signal of up to ~0.5 mm/yr at far-field continental shorelines and in the middle of ocean basins (Mitrovica and Milne, 2002). In the former region, the sign of the levering signal will depend on the detailed path of the shoreline relative to the geometry of crustal tilting. In equatorial ocean basins, the total syphoning signal has driven a sea-level fall that is responsible for the ubiquitous emergence of islands and ancient corals over the past few thousand years (Pirazzoli et al., 1988; Dickinson, 2004). It is important to emphasize that this geographic variability in sea level described above has occurred over a period of the last 3–4 millennia in which GMSL has experienced little, if any change.

As one example of the relevance of sea-level physics to archaeology, a combination of syphoning and levering is responsible for a southeastern migration of the shoreline at the northern edge of the Persian Gulf over the last few thousand years. Lambeck (1996b) highlights the insights that can be gained by abandoning the "bathtub" model in this case in favor of more physically realistic reconstructions of sea level. A eustatic approximation would predict no change in shoreline position near the Persian Gulf, whereas models of the GIA process predict a sea-level fall of several meters. This migration places the reconstructed shoreline close to ancient Neolithic settlements that are presently hundreds of kilometers from the Persian Gulf.

4. Methods: sea-level modeling

Sea-level change is analogous to the negative of topography change. Thus, we reconstruct paleotopography by adding the change in sea level between the time period of interest and the present day to a data set of present-day topography (Ryan et al., 2009). In the "bathtub" model, the quantity we add to present-day topography is assumed to be uniform across the globe and equal to the change in eustatic (or global mean) sea level.

As discussed in Section 3, more accurate reconstructions must account for the geographic variability in ice age sea-level change associated with the effects of GIA. For this purpose, we adopt the generalized,

pseudo-spectral sea-level theory described in Kendall et al. (2005), which is based on viscoelastic Love number theory (Peltier, 1974). The theory accounts for viscoelastic deformation of the solid Earth, and associated perturbations to both the gravitational field and rotational state driven by mass redistribution, and it incorporates an exact expression for shoreline migration in the evolving Earth system. We neglect thermosteric effects (i.e., thermal expansion) on sea level, as well as the impact of ocean tides and changes in ocean circulation. The mathematical equations that govern the sea-level theory and the iterative, pseudo-spectral algorithm used to solve them are comprehensively described in Section 3 and Appendix A of Kendall et al. (2005).

Our numerical simulations require, as input, models for both the viscous and elastic structure of the solid Earth, which we assume varies with depth alone, and the geometry of ice mass changes. We use a viscosity model characterized by a high viscosity lithosphere of thickness 96 km, and an order of magnitude increase in the viscosity from the shallow to deep mantle (these viscosities are, respectively, 5×10^{20} Pa s and 5×10^{21} Pa s). This model is within the class of viscosity profiles preferred by a number of independent studies of GIA data sets (e.g., Mitrovica and Forte, 2004; Lambeck et al., 2014). The elastic structure of the Earth has been mapped by seismological studies of which we adopt the widely used Preliminary Reference Earth Model (Dziewonski and Anderson, 1981). Each simulation of the GIA process, based on coupling of the above Earth model with an ice history, yields the spatial geometry of sea-level change across the last glacial cycle.

5. Results & discussion

5.1. Sunda and Sahul

To consider the potential importance of updated GMSL histories and accurate sea-level modeling to assessments of ancient migration routes, we focus in this section on the migration from Sunda to Sahul. We emphasize that this case study is intended to be illustrative rather than comprehensive since we only consider the impact of sea-level physics beyond the "bathtub" and the new constraints on GMSL. From a geophysical perspective, a comprehensive analysis of the relative feasibility of different routes would additionally require reconstructions of ocean currents, winds, and ancient landscapes, as well as the consideration of tectonic deformations. These factors – as well as issues related to resources, technological innovation, and human motivation - are beyond the scope of the present study but will be treated in a future assessment of the suite of possible routes from Sunda to Sahul in the rapidly evolving Earth system of the Last Glacial Period.

The present-day region encompassing Australia and Indonesia comprised Sunda to the northwest and Sahul to the southeast during sea-level lowstands throughout geologic history. Today, the shallow coastal shelves within these regions include an abundance of islands that have been exposed and inundated throughout the Plio-Pleistocene ice age (the last 3 Myr). The shallow nature of the local topography requires highly accurate regional sea-level modeling, as small changes in reconstructed sea level can create vastly different paleoenvironments and exposed areas of land (Pico et al., 2020).

The timing of initial human migration from Sunda into Sahul remains debated – it is thought to have occurred between ~65 and 45 ka, and the earliest, although contested, evidence of human occupation in Northern Australia is from stone tool assemblages in Madjedbebe rock shelter dated to 65 ka (Clarkson et al., 2017; O'Connell et al., 2018). We furthermore acknowledge the Indigenous oral histories that maintain that they have been on the continent "with the first sunrise" (Munro, 2008, p. 4). Assuming initial migration during the Late Pleistocene, the movement of ancient *Homo sapiens* into Sahul would constitute the first known long-range human migration by sea, but the exact path and timing is unknown. Migrants likely moved from island to island (potentially incrementally across tens to thousands of years) using either bamboo rafts or other sailing craft (Balme, 2013; see also Irwin, 1994; Kingdon, 1993; Anderson, 2018). The routes taken, whether over shorter time periods or over an extended dispersal stage, were both limited and defined physically by factors listed above, including local oceanography (e.g., surface currents), ground-level winds, island resources, and sea-level change.

In the following analysis, we reconstruct sea level and shoreline positions at two times that bound the above range, 46 ka and 64 ka, and also consider, as illustrative examples, the implications of these reconstructions for the total length of ocean travel along both a northern and southern migration route suggested by Birdsell (1977).

Reconstructing paleotopography or paleo-shorelines requires knowledge of sea level in the past relative to today. This is straightforward in the case of the "bathtub" assumption. From Fig. 1, at 46 ka, the ICEPC2 and LC01 models are characterized by GMSL of −37 m and −58 m, respectively. Thus, under the "bathtub" assumption, topography at 46 ka would be reconstructed by simply adding a constant 37 m or 58 m to present-day topography for these two models. An accurate reconstruction of paleotopography, however, requires that a correction be made for the geographically variable effects of GIA on sea level in addition to other local uncertainties. Fig. 3 presents the GIA-induced change in sea level from 46 ka to present-day, calculated using the ICEPC2 ice history. As previously noted, this sea-level change is equivalent to the *negative* of topography change from 46 ka to present, and thus it is precisely the correction to the "bathtub" reconstruction of topography at 46 ka to account for the GIA process. That is, the global topography at 46 ka would be reconstructed by adding 37 m to present day topography and then adding the GIA field shown in Fig. 3.

Fig. 3A illustrates the global variability of the GIA signal. At 46 ka, ocean mass is gravitationally pulled toward the region covered by ice sheets (Canada, Scandinavia, the Antarctic) and the bedrock beneath the ice sheets is depressed (Fig. 2D; left). From 46 ka to the present-day, most of this ice (besides the Antarctic) disappears, causing water to migrate away from these locations due to the weakening gravitational pull (Fig. 2D, right) and rebound of the crust (Fig. 2E). This drives a sea-level fall of up to hundreds of meters from 46 ka to present day (the dark blue over North America, Scandinavia, and Antarctica in Fig. 3A are off the color bar scale). That is, moving forward in time, the topography is increasing in this area. Thus, as described above, to estimate topography at 46 ka one would add the signal in Fig. 3A to the "bathtub" reconstruction of topography.

In the region at the periphery of these zones of ancient ice cover, two competing effects combine to drive sea-level change from 46 ka to present day. The first is the subsidence of the peripheral bulge between 46 ka and present (Fig. 2E), which drives a sea-level rise. The second is the migration of water away from these areas due to the weakening gravitational attraction of the diminished ice sheet, which contributes a sea-level fall (Fig. 2D, right). Just outside the ice perimeter, the subsidence of the peripheral bulge dominates the gravitational effect and there is a net sea-level rise of magnitude tens of meters from 46 ka to present day (the red zones that encircle previous ice cover; Fig. 3A) due to GIA. Thus, the GIA correction to a "bathtub" reconstruction of topography at 46 ka is positive at these sites. Beyond these zones at the perimeter of ancient ice cover, gravitational effects on sea level (plus a continental levering signal over the southern US and Mexico; darker blue near continental coastlines in Fig. 3A) dominate peripheral bulge subsidence and the net effect is a GIA-induced sea-level fall of tens of meters from 46 ka to present day (e.g., blue regions encircling red, across the United States; Fig. 3A), and thus an increase in topography of the same magnitude. The GIA correction to the "bathtub" reconstruction of topography is, in this case, negative.

In the far-field of the ice sheet, including our study region, three major GIA effects lead to a complex geometry of sea-level change. First, the diminished gravitational pull associated with a reduction in global ice masses leads to a migration of water into the far-field and a sea-level rise (Fig. 2D, right). Second, a net subsidence of the peripheral bulges encircling ancient ice cover from the glacial period to present syphons

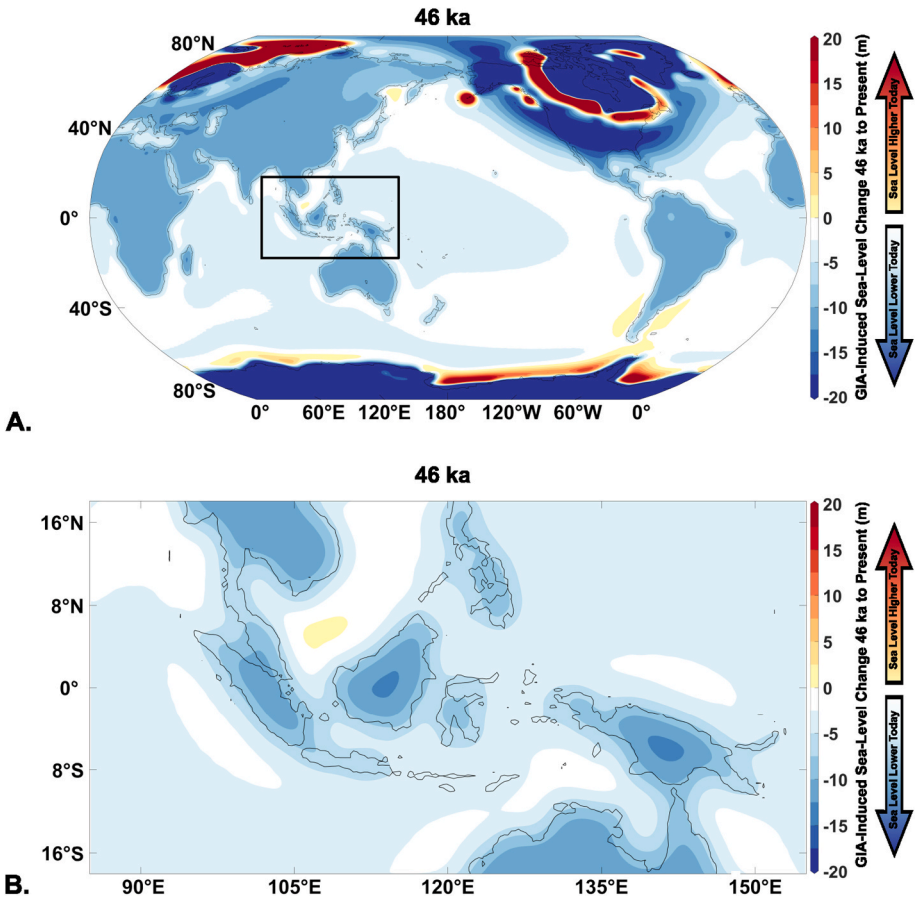

Fig. 3. GIA-induced change in sea level from 46 ka to present day. A. Global map of the GIA-induced sea-level change computed using a gravitationally self-consistent sea-level theory (see Section 3). The calculation is based on the ICEPC2 ice history (described in Section 2) and viscoelastic Earth model described in Section 3. The black box outlines our region of study within Sunda and Sahul. **B.** Close-up of frame (A) within our region of study. Note that this field is equivalent to the correction that should be applied to a reconstruction of topography at 46 ka based on the "bathtub" model in order to account for the effects of GIA (Section 5.1).

water away from the far-field (Fig. 2E, at right) and contributes a sea-level fall. Third, continental levering due to ocean loading contributes a sea-level rise offshore and fall onshore from the glacial period to present (Fig. 2F). Because the present-day ocean load is greater than at 46 ka, the levering-induced crustal subsidence (sea-level rise) offshore, and crustal uplift (sea-level fall) onshore, shown in Fig. 2F, is more advanced at present than during the glacial period. The net effect of these three GIA processes is a variable far-field sea-level fall (or rise in topography) of magnitude up to ~10 m between 46 ka and the present day.

The same sea-level physics evident in Fig. 3 would be active in the case of the globally variable sea-level change from 64 ka to present-day, albeit with different amplitudes given that the GMSL (and ice volume) change over the past 64 ka is greater than the past 46 ka (63 versus 37 m; Fig. 1). In particular, the GIA process would once again contribute a sea-level fall within the far field.

The top panels of Fig. 4 show the difference in the reconstructed location of shorelines at 46 ka in the Sunda and Sahul region for four different sea-level simulations. Fig. 4A and C include results based on the "bathtub" assumption of sea-level change for LC01 and ICEPC2, as well as a reconstruction for ICEPC2 including GIA. Fig. 4B and D reproduce A and C but replace the LC01 results with the "bathtub" assumption applied to the ICE-5G ice history. The GMSL rise between 46 ka and the present-day is ~21 m greater in the case of LC01 relative to ICEPC2 (58 m versus 37 m; Fig. 1). Accordingly, the former model yields significantly more shoreline migration across the past 46 kyr than the latter – the difference (~1 million km^2) is shown as the purple region on Fig. 4A. The difference in ocean area at 46 ka between the two simulations based on the ICEPC2 ice history – i.e., "bathtub" assumption or full GIA modeling (Fig. 3) – is ~0.4 million km^2 (orange region; Fig. 4A). There is less shoreline migration when GIA effects are included because, as previously noted, GIA acts against the GMSL rise predicted for this region (i.e., contributes a sea-level fall) from 46 ka to present day using the "bathtub" assumption (i.e., 37 m) by up to ~10 m (Fig. 3). The same trends are evident in Fig. 4B, although in this case the shoreline migration computed using the ICE-5G "bathtub" simulation is more extensive than the analogous LC01 simulation, which reflects the even larger GMSL change across the last 46 kyr of the former ice history relative to the latter (90 m versus 58 m; Fig. 1).

The bottom panels of Fig. 4 show reconstructed shorelines at 64 ka. Regarding simulations based on the "bathtub" assumption, ICE-5G once again shows the largest exposed land, followed by ICEPC2 and LC01. The order of the latter two in Fig. 4C is reversed relative to Fig. 4A, which reflects the GMSL change associated with these models since 64 ka (63 m versus 55 m, respectively; Fig. 1). Once again, introducing GIA effects in the ICEPC2 reconstruction reduces the amount of shoreline migration by contributing a sea-level fall since 64 ka that acts against the GMSL rise of 63 m over the same period.

5.2. Sea-level model comparison and consequences for migration

Our updated reconstruction has significant implications for sea-level changes at specific sites. As an example, Fig. 5 shows the predicted change in topography over time relative to present day at Asitau Kuru, a near-coastal archaeological site in modern-day East Timor with evidence of human occupation at 44 ka (O'Connor, 2007; Shipton et al., 2019). During the likely period of initial migration into Australia (~65,000–45,000 years ago), the updated (ICEPC2) history departs from the LC01 "bathtub" prediction by up to ~20 m and the ICE-5G "bathtub" prediction by up to ~50 m, a pattern that mirrors the discrepancy in the GMSL change of the models over this window of time. Once again, the incorporation of an accurate sea-level prediction acts in opposition to

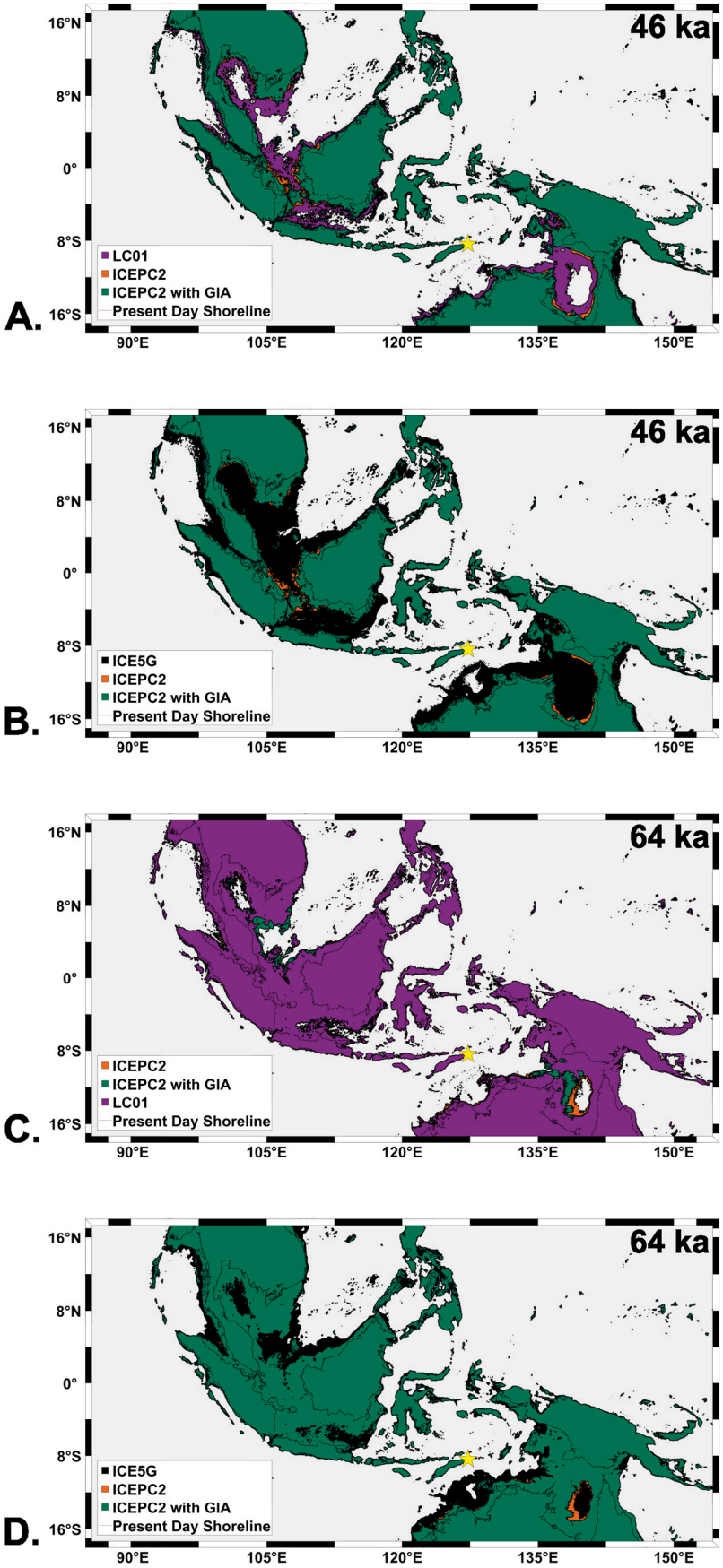

Fig. 4. Reconstruction of migrating shorelines. **A.** Land cover at 46 ka in the Sunda/Sahul region computed from simulations based on the "bathtub" sea-level assumption with either the LC01 (purple land mask) or ICEPC2 (orange land mask) ice history, and the ICEPC2 ice history with a gravitationally self-consistent sea-level calculation of the GIA signal (green land mask). **B.** As in A, except showing land cover computed with the ICE-5G ice history and the "bathtub" assumption (black land mask) instead of LC01. **C.** As in A, except for land cover at 64 ka. **D.** As in B, except for land cover at 64 ka. The yellow star in each panel indicates the location of Asitau Kuru cave, the archaeological site adopted in Fig. 5. Topography created using GMRT (Ryan et al., 2009). (For interpretation of the references to color in this figure legend, the reader is referred to the Web version of this article.)

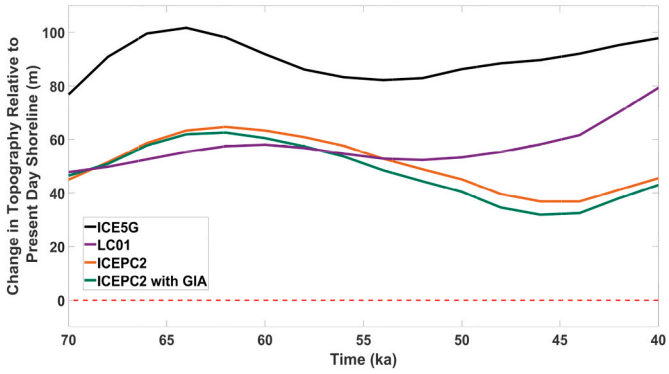

Fig. 5. Variation of topography. Change of topography relative to present day at the Asitau Kuru cave archaeological site in East Timor, 8.4°N, 127.3°E (O'Connor, 2007; Figs. 3B and 4) in four different model simulations (as labeled). This site is relevant for studies of the human migration from Sunda into Sahul, which is thought to have occurred between 65 and 45 ka.

the GMSL rise between 46 ka and the present in this region (Fig. 3B) and the net result is that the discrepancy between the commonly used LC01 and ICE-5G simulations and the "updated" ICEPC2 simulation increases by an additional ~5 m at Asitau Kuru when the "bathtub" assumption is abandoned in the latter.

As a simple illustration of the impact of recent revisions to the GMSL curve and the incorporation of sea-level physics, we will use the above calculations to consider the total distance travelled by sea from Sunda to Sahul for southern route 2A and northern route 1B (Birdsell, 1977; Kealy et al., 2018) for each paleo-shoreline simulation at 46 ka and 64 ka (Table 1). As one would expect, for both epochs, the distance travelled by sea increases as the extent of the exposed land reconstructed in the simulations (Fig. 4) decreases. At 46 ka, this ordering is ICE5G, LC01, and ICEPC2 ("bathtub" models), and finally the ICEPC2 simulation with GIA. Across these simulations the distance increases by 167 km (50%) for the northern route and 123 km (22%) for the southern route. At 64 ka, the ordering is rearranged such that both ICEPC2 simulations are characterized by a total distance that is intermediate to the ICE5G and LC01 simulations, with a range of 72 km (23%) for the northern route and 89 km (17%) for the southern route.

Our updated paleoshoreline reconstructions have the potential to impact the viability of proposed migration routes (e.g., Birdsell, 1977; recently reviewed by Norman et al., 2018; see also Allen and O'Connell, 2020), and archaeological evidence for human uses of the area and subsistence-related reasons for migration (e.g., O'Connell et al., 2010; O'Connell and Allen, 2012). For example, if the migration from Sunda to Sahul occurred at 46 ka, the passageway between Sumatra, Java, and Borneo opens significantly when adopting ICEPC2, and a less contiguous landmass is present in the Sahul region. The resulting topography has more open ocean, and thus greater distances between the islands. The latest "bathtub" models show preference for the northern route (e.g., Norman et al., 2018; Kealy et al., 2018; Bird et al., 2019). However, at 46 ka, this preference would be complicated by the requirement of sea travel between mainland southeast Asia and Borneo predicted with the ICEPC2 ice history. Overall, the region immediately surrounding Borneo is sensitive to slight changes in predicted sea level, an important consideration given that the area is the starting point for routes from Sunda to Sahul. To emphasize the importance of specific island distances to the totals in Table 1, individual island-to-island distances associated with these totals are listed in Table S1.

Changes in island topography also affect island-to-island intervisibility, a central factor in determining most likely pathways. A pathway across a body of water to an unknown location is more likely to be successful if the target landmass is visible from the landmass travelers depart from, or if the target landmass becomes visible before migrants lose sight of the departure shoreline (Kealy et al., 2017). The routes proposed by Birdsell (1977) rely on land exposure for greater intervisibility between islands to aid in migration, and in our model, at certain times, some land crossings become more difficult, if not impossible.

As we noted in the introduction, we do not consider here the impact of other, highly localized processes on sea level such as tectonics or sedimentation and erosion. To explore the sensitivity of the route distances to spatially localized perturbations in sea level, we performed two tests (repeated five times each) in which we computed the impact of subtracting random fields of topography within the region to distances along routes 1B and 2A. In the first test, this field varied from −20 m to 20 m and the route distances were perturbed by roughly −1 and −12 km on average, respectively. Next, to consider the possibility of a systematic bias associated with tectonics and sedimentation, a topography field that varied from 0 to 20 m (i.e., a mean uplift across the region of ~10 m) was applied and in this case, distances were on average increased by about 14 km for route 1B and 31 km for 2A. This change in route distance is smaller than the impact from adopting the new GMSL curve associated with ICEPC2 ice history and is comparable to the impact of GIA on these distances (Table 1). These simple tests provide a measure of the potential importance of these local processes for future investigations of the routes taken by early humans as they migrated from Sunda to Sahul.

5.3. *Post-LGM sea-level rise at the Strait of Dover*

Updates in the GMSL curve dominate the variation in route distances evident in Table 1 and reflect the large uncertainties in the GMSL curve prior to LGM. While this initial case study highlights the importance of the adopted GMSL curve, as a second case study we briefly consider predictions of sea-level rise (lowering of topography) at the Strait of Dover in the post-LGM period, a time window across which the GMSL curve has been better constrained and the significance of GIA effects is highlighted. The English Channel is thought to have been formed by a series of megafloods (Gibbard, 2007; Gupta et al., 2007) and a land connection between Britain and continental Europe was intermittently flooded and exposed through subsequent ice age cycles. This region also carries relevance for studies of human settlement patterns, as the area was likely a hub for resources, hunting and gathering, communication, and sea travel when it was periodically exposed (and not covered by ice sheets) going back to the late Pleistocene (Coles, 1998, 2000; Gaffney and Thomson, 2007; Bailey et al., 2020). Similar to the Sunda and Sahul region, Doggerland (the region encompassing the now-submerged connection between Britain and continental Europe) is shallow and therefore sensitive to slight changes in sea level. The most recent flooding of the Doggerland region occurred near the end of the last

Table 1
Distance travelled (in km) by sea from Sunda to Sahul via Birdsell's (1977) northern and southern routes (specific routes from Kealy et al., 2017) for different reconstructions of topography. For both 46 ka and 64 ka, the first three cases are the "bathtub" assumptions. These values assume no ocean currents and do not include land travel distances. Supplementary Table 1 decomposes these totals into individual island-to-island distances for each route.

Topography	Northern Route 1B (km)	Southern Route 2A (km)
46 ka		
ICE5G eustatic	333	572
LC01 eustatic	372	617
ICEPC2 eustatic	478	672
ICEPC2 eustatic	478	672
ICEPC2 with GIA	500	695
64 ka		
ICE5G eustatic	311	528
LC01 eustatic	383	617
ICEPC2 eustatic	367	606
ICEPC2 eustatic	367	606
ICEPC2 with GIA	372	606

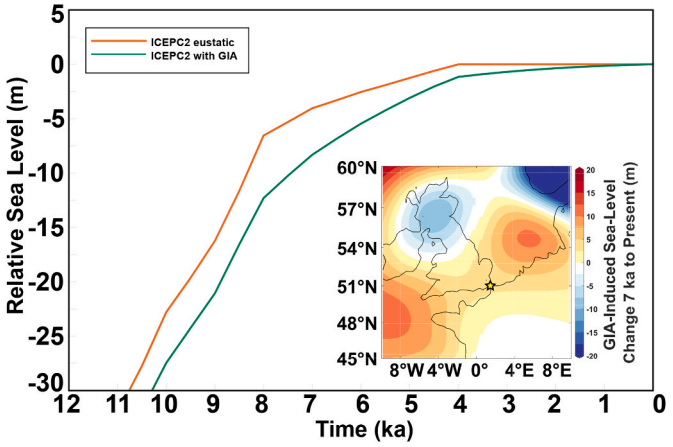

Fig. 6. Holocene Sea-Level Change at the Strait of Dover. Prediction of relative sea-level change over the past 12 kyr based on either (orange line) the "bathtub" (eustatic) model, or (green line) GIA modeling at a site in the middle of the strait (see star in inset). Inset – map of the GIA-induced change in sea level from 7 ka to present-day; the eustatic contribution to the total sea-level change has been removed. In all cases the ICEPC2 ice history is adopted. (For interpretation of the references to color in this figure legend, the reader is referred to the Web version of this article.)

deglacial phase, at ~8.2 ka (Weninger et al., 2008).

To consider how the timing of the flood event was impacted by GIA processes, Fig. 6 shows predictions of relative sea-level change at a site in the center of the Strait of Dover, the 33 km wide waterway between Britain and France. We note that previous studies have considered the GIA signal over the broader region of Doggerland, with an emphasis on geographic variability (Sturt et al., 2013; Spada and Galassi, 2017). Fig. 6 shows relative sea-level predictions based on the "bathtub" model (orange) and GIA modeling (green) at a site in middle of the strait (Fig. 6, inset). Both predictions are based on the ICEPC2 history. The inset on the figure shows a map of the sea-level change over the region from 7 ka to present, after removal of the eustatic signal. The net effect of GIA across the English Channel is a rise in sea level that is due to crustal subsidence at the periphery of both the Fennoscandian and British Isles Ice Sheets (Fig. 2E) and additional crustal subsidence due to ocean load-induced continental levering (Fig. 2F). The latter is evident in the down-toward-the-ocean crustal tilting (and increased sea-level rise) both north and south of the English Channel. These subsidence signals continued through the Late Holocene to present-day. We note that the choice of Earth and ice model (e.g., ICE-5G, ICEPC2, etc.) will affect the magnitude of the predicted signal.

The net effect is that the "bathtub" assumption would predict far earlier flooding of the Strait of Dover than the full GIA theory. The timing of the breach may also have implications for human-landscape interactions, limiting the type of potential land use (e.g., primarily marine, or agricultural; Ward et al., 2006) once the region became sufficiently inundated (though we note that the people of Doggerland likely adapted to rising sea level until land use became untenable; Coles, 2000).

6. Conclusions

We have demonstrated the importance of using state-of-the-art sea-level models that incorporate the most recent constraints on past GMSL and ice geometry and accurate modeling of the GIA process in reconstructing paleotopographies for various studies, including archaeological research on human migration. The differences between our model of sea-level change and the "bathtub" model have the potential to significantly impact the emergence and flooding of ancient landscapes, and therefore human movement and interaction. These ancient landscapes ultimately governed many aspects of human migration and the use of coastal environments, including the timing, methodology, and viability for habitation. Accurate modeling of paleo sea level, and the resulting paleoenvironmental reconstructions, are essential for a rigorous assessment of the routes, timing, and habitability of migration and environmental models in Sunda and Sahul, the Strait of Dover, and beyond.

Future work will expand on the improvements highlighted here to include simulations of paleo-ocean currents and a consideration of possible vertical motion due to dynamic topography and tectonics (e.g., Austermann et al., 2013). We suggest that incorporating gravitationally self-consistent sea level, high-resolution paleotopography, and simulated paleo-ocean currents should define future "best practices" for modeling studies aimed at accurately determining ocean migration routes and human-paleoenvironmental interactions. The case studies considered in this article are meant to be illustrative, but the principles presented here can be applied to a range of archaeological research involving paleogeography (e.g., paleolithic seafaring in the Mediterranean; the occupation of Flores by *Homo floresiensis*; migration through and/or around the Red Sea; etc.). The interface between sea-level research, physical oceanography, paleoclimatology, and archaeology has great potential for deepening our understanding of both the modern and ancient world, as well as our ancestors that moved through these spaces.

Declaration of competing interest

Declarations of interest: none.

Acknowledgements & Data Availability

We acknowledge support from the Dean's Competitive Fund for Promising Scholarship, Faculty of Arts and Science, Harvard University (M.J.B., J.X.M.). T.P. acknowledges funding from NSF EAR Postdoctoral Fellowship and UC President's Postdoc Fellowship Program. We thank the editor and the four anonymous reviewers for their constructive advice in regards to earlier versions of this manuscript. Researchers desiring regional paleotopographic maps for their studies are welcome to email the authors requesting a reconstruction. Usage of sea-level physics illustrations is permitted with appropriate citation of this publication and the artist, Maximilian Werner.

Glossary of terms

Term	*Definition*
GMSL	Global mean sea level. Global sea-level height averaged over ocean area at a given time, sometimes used interchangeably with the term "eustatic" sea level. Referred to here as the "bathtub" model of sea-level change.
GIA	Glacial isostatic adjustment. Earth's gravitational, deformational, and rotational response to changing ice and ocean surface loads across an ice age.
LIG	Last Interglacial. The period ~129,000-117,000 years ago during which grounded ice sheets had retreated to minimum extent between glacial cycles.
LGM	Last Glacial Maximum. The period ~26,000-20,000 years ago during the last glacial cycle during which ice sheets were at their maximum extent and volume.
RSL	Relative sea level. Sea level at any time in the past relative to present-day sea level. A negative RSL corresponds to a lower sea level at a site than present day. A positive RSL corresponds to a higher sea level at a site than present day.
LC01	Global mean sea-level curve from Lambeck and Chappell (2001). This curve is constructed from analyses of geological evidence of past sea level, including coral reefs, sediments, peats, and tree roots.

ICE-5G ICE-5G ice history and affiliated sea-level curve from Peltier and Fairbanks (2006). In the period prior to LGM, this curve is largely based on oxygen isotope records from the South Indian ocean. In the post-LGM period, the ice history was constructed from an analysis of geological records.

ICEPC2 ICEPC2 ice history and affiliated sea-level curve from Pico et al. (2017). This ice history was constructed as a revision to ICE-5G based on sediment core records from the South China Sea and sea-level markers along the US East Coast, including tidal, estuarine, and marine lithofacies. This history mainly modifies peak GMSL at 44 ka from earlier models to be significantly higher (i.e., less ice volume).

Appendix A. Supplementary data

Supplementary data to this article can be found online at https://doi.org/10.1016/j.jas.2021.105507.

References

Allen, J., O'Connell, J.F., 2020. A different paradigm for the initial colonisation of Sahul. Archaeol. Ocean. 55, 1–14. https://doi.org/10.1002/arco.5207.

Anderson, A., 2018. Ecological contingency accounts for earliest seagoing in the western Pacific Ocean. J. I. Coast Archaeol. 13, 224–234.

Austermann, J., Mitrovica, J.X., Latychev, K., Milne, G.A., 2013. Barbados-based estimate of ice volume at Last Glacial Maximum affected by subducted plate. Nat. Geosci. 6, 553–557.

Bailey, G., Momber, G., Bell, M., Tizzard, L., Hardy, K., Bicket, A., Tidbury, L., Benjamin, J., Hale, A., 2020. Great Britain: the intertidal and underwater archaeology of Britain's submerged landscapes. In: The Archaeology of Europe's Drowned Landscapes. Springer, Cham, pp. 189–219.

Balme, J., 2013. Of boats and string: the maritime colonisation of Australia. Quat. Int. 285, 68–75.

Bird, M.I., Condie, S.A., o'Connor, S., o'Grady, D., Reepmeyer, C., Ulm, S., Zega, M., Saltré, F., Bradshaw, C.J., 2019. Early human settlement of Sahul was not an accident. Sci. Rep. 9, 1–10.

Birdsell, J.B., 1977. The recalibration of a paradigm for the first peopling of Greater Australia. Sunda and Sahul: Prehistoric Studies in Southeast Asia, Melanesia, and Australia 113–167.

Clark, J., Mitrovica, J.X., Alder, J., 2014. Coastal paleogeography of the California–Oregon–Washington and Bering Sea continental shelves during the latest Pleistocene and Holocene: implications for the archaeological record. J. Archaeol. Sci. 52, 12–23.

Clarkson, C., Jacobs, Z., Marwick, B., Fullagar, R., Wallis, L., Smith, M., Roberts, R.G., Hayes, E., Lowe, K., Carah, X., Florin, S.A., McNeil, J., Cox, D., Arnold, L.J., Hua, Q., Huntley, J., Brand, H.E.A., Manne, T., Fairbairn, A., Shulmeister, J., Lyle, L., Salinas, M., Page, M., Connell, K., Park, G., Norman, K., Murphy, T., Pardoe, C., 2017. Human occupation of northern Australia by 65,000 years ago. Nature 547, 306–310.

Coles, Bryony J., 1998. Doggerland: A Speculative Survey. In: Proceedings of the Prehistoric Society, 64. Cambridge University Press, pp. 45–81.

Coles, Bryony, 2000. Doggerland: the cultural dynamics of a shifting coastline. Geol. Soc. London, Spec. Publ. 175 (1), 393–401. https://doi.org/10.1144/GSL.SP.2000.175.01.27.

Creveling, J.R., Mitrovica, J.X., Clark, P.U., Waelbroeck, C., Pico, T., 2017. Predicted bounds on peak global mean sea level during marine isotope stages 5a and 5c. Quat. Sci. Rev. 163, 193–208.

Dahlen, F.A., Tromp, J., 1998. Theoretical Global Seismology. Princeton University Press, Princeton, NJ, p. 944.

Dalton, A.S., Finkelstein, S.A., Barnett, P.J., Forman, S.L., 2016. Constraining the late Pleistocene history of the Laurentide ice sheet by dating the Missinaibi formation, Hudson Bay lowlands, Canada. Quat. Sci. Rev. 146, 288–299. https://doi.org/10.1016/j.quascirev.2016.06.015.

Dalton, A.S., Finkelstein, S.A., Forman, S.L., Barnett, P.J., Pico, T., Mitrovica, J.X., 2019. Was the Laurentide ice sheet significantly reduced during marine isotope stage 3? Geology 47, 111–114. https://doi.org/10.1130/G45335.1.

Dickinson, W.R., 2004. Impacts of eustasy and hydro-isostasy on the evolution and landforms of Pacific atolls. Palaeogeogr. Palaeoclimatol. Palaeoecol. 213, 251–269. https://doi.org/10.1016/j.palaeo.2004.07.012.

Dobson, J.E., Spada, G., Galassi, G., 2020. Global choke points may link sea level and human settlement at the Last Glacial Maximum. Geogr. Rev.

Dziewonski, A.M., Anderson, D.L., 1981. Preliminary reference Earth model. Phys. Earth Planet. In. 25, 297–356.

Farrell, W.E., Clark, J.A., 1976. On postglacial sea level. Geophys. J. Int. 46, 647–667.

Fedje, D.W., Josenhans, H., 2000. Drowned forests and archaeology on the continental shelf of British Columbia, Canada. Geology 28, 99–102. https://doi.org/10.1130/0091-7613(2000)28<99:DFAAOT>2.0.CO;2.

Gaffney, V.L., Thomson, K., Fitch, S., 2007. Mapping Doggerland: the mesolithic landscapes of the southern north sea. Archaeopress.

Gibbard, P., 2007. Europe cut adrift. Nature 448, 259–260. https://doi.org/10.1038/448259a.

Gupta, S., Collier, J.S., Palmer-Felgate, A., Potter, G., 2007. Catastrophic flooding origin of shelf valley systems in the English Channel. Nature 448, 342–345. https://doi.org/10.1038/nature06018.

Hoffecker, J.F., Elias, S.A., O'Rourke, D.H., Scott, G.R., Bigelow, N.H., 2016. Beringia and the global dispersal of modern humans. Evol. Anthropol. Issues News Rev. 25, 64–78.

Irwin, G., 1994. The Prehistoric Exploration and Colonisation of the Pacific. Cambridge University Press.

Kealy, S., Louys, J., O'Connor, S., 2018. Least-cost pathway models indicate northern human dispersal from Sunda to Sahul. J. Hum. Evol. 125, 59–70.

Kealy, S., Louys, J., O'Connor, S., 2017. Reconstructing palaeogeography and inter-island visibility in the Wallacean archipelago during the likely period of Sahul colonization, 65–45 000 Years ago. Archaeol. Prospect. 24, 259–272. https://doi.org/10.1002/arp.1570.

Kendall, R.A., Mitrovica, J.X., Milne, G.A., 2005. On post-glacial sea level–II. Numerical formulation and comparative results on spherically symmetric models. Geophys. J. Int. 161, 679–706.

Kingdon, J., 1993. Self-made Man: Human Evolution from Eden to Extinction. John Wiley & Sons Incorporated.

Kuijjer, E.K., 2020. The Role of Open Ocean and Coastal Tidal Currents in the Maritime Migration to Sahul, Ca, 65. University of Southampton, 000-50,000 years ago (PhD Thesis).

Lambeck, K., 1996a. Sea-level change and shore-line evolution in Aegean Greece since Upper Palaeolithic time. Antiquity 70, 588–611.

Lambeck, K., 1996b. Shoreline reconstructions for the Persian Gulf since the last glacial maximum. Earth Planet Sci. Lett. 142, 43–57. https://doi.org/10.1016/0012-821X(96)00069-6.

Lambeck, K., Chappell, J., 2001. sea level change through the last glacial cycle. Science 292, 679–686. https://doi.org/10.1126/science.1059549.

Lambeck, K., Purcell, A., Flemming, N.C., Vita-Finzi, C., Alsharekh, A.M., Bailey, G.N., 2011. Sea level and shoreline reconstructions for the Red Sea: isostatic and tectonic considerations and implications for hominin migration out of Africa. Quat. Sci. Rev. 30, 3542–3574.

Lambeck, K., Rouby, H., Purcell, A., Sun, Y., Sambridge, M., 2014. sea level and global ice volumes from the last glacial maximum to the Holocene. Proc. Natl. Acad. Sci. Unit. States Am. 111, 15296–15303.

Lin, Y., Hibbert, F.D., Whitehouse, P.L., Woodroffe, S.A., Purcell, A., Shennan, I., Bradley, S.L., 2021. A reconciled solution of Meltwater Pulse 1A sources using sea-level fingerprinting. Nat. Commun. 12, 1–11.

Lisiecki, L.E., Raymo, M.E., 2005. A Pliocene-Pleistocene stack of 57 globally distributed benthic δ18O records. Paleoceanography 20.

Liu, J., Milne, G.A., Kopp, R.E., Clark, P.U., Shennan, I., 2016. Sea-level constraints on the amplitude and source distribution of Meltwater Pulse 1A. Nat. Geosci. 9, 130–134.

Martinson, D.G., Pisias, N.G., Hays, J.D., Imbrie, J., Moore, T.C., Shackleton, N.J., 1987. Age dating and the orbital theory of the ice ages: development of a high-resolution 0 to 300,000-year chronostratigraphy 1. Quat. Res. 27, 1–29.

Milne, G.A., Mitrovica, J.X., 2008. Searching for eustasy in deglacial sea-level histories. Quat. Sci. Rev. 27, 2292–2302.

Mitrovica, J.X., Forte, A.M., 2004. A new inference of mantle viscosity based upon joint inversion of convection and glacial isostatic adjustment data. Earth Planet Sci. Lett. 225, 177–189.

Mitrovica, J.X., Milne, G.A., 2002. On the origin of late Holocene sea-level highstands within equatorial ocean basins. Quat. Sci. Rev. 21, 2179–2190.

Mitrovica, J.X., Hay, C.C., Kopp, R.E., Harig, C., Latychev, K., 2018. Quantifying the sensitivity of sea level change in coastal localities to the geometry of polar ice mass flux. J. Clim. 31, 3701–3709.

Mitrovica, J.X., Peltier, W.R., 1991. On postglacial geoid subsidence over the equatorial oceans. J. Geophys. Res.: Solid Earth 96, 20053–20071.

Munro, Jenny, 2008. Bo-rä-ne Ya-goo-na Par-ry-boo-go = Yesterday Today Tomorrow: an aboriginal history of Willoughby. Interview by Jessica Currie. Willoughby City Council, p. 4.

Nakada, M., Lambeck, K., 1989. Late Pleistocene and Holocene sea-level variations in Australian region and mantle rheology. Geophys. J. Int. 96, 497–517.

Norman, K., Inglis, J., Clarkson, C., Faith, J.T., Shulmeister, J., Harris, D., 2018. An early colonisation pathway into northwest Australia 70-60,000 years ago. Quat. Sci. Rev. 180, 229–239.

O'Connell, JamesF., Allen, J., 2012. The restaurant at the end of the universe: modelling the colonisation of Sahul. Aust. Archaeol. 74, 5–31. https://doi.org/10.1080/03122417.2012.11681932.

O'Connell, J.F., Allen, J., Hawkes, K., 2010. Pleistocene Sahul and the origins of seafaring. The global origins and development of seafaring 57–68.

O'Connell, J.F., Allen, J., Williams, M.A.J., Williams, A.N., Turney, C.S.M., Spooner, N. A., Kamminga, J., Brown, G., Cooper, A., 2018. When did Homo sapiens first reach Southeast Asia and Sahul? Proc. Natl. Acad. Sci. U.S.A. 115, 8482–8490. https://doi.org/10.1073/pnas.1808385115.

O'Connor, S., 2007. New evidence from East Timor contributes to our understanding of earliest modern human colonisation east. I of the Sunda Shelf I 14.

Peltier, R., 1982. Dynamics of the ice age Earth. Adv. Geophys. 24, 1–146.

Peltier, W.R., 1974. The impulse response of a Maxwell Earth. Rev. Geophys. 12, 649–669. https://doi.org/10.1029/RG012i004p00649.

Peltier, W.R., Fairbanks, R.G., 2006. Global glacial ice volume and Last Glacial Maximum duration from an extended Barbados sea level record. Quat. Sci. Rev. 25, 3322–3337.

Pendea, I.F., Costopoulos, A., Nielsen, C., Chmura, G.L., 2010. A new shoreline displacement model for the last 7 ka from eastern James Bay, Canada. Quat. Res. 73, 474–484.
Pico, T., 2020. Towards assessing the influence of sediment loading on Last Interglacial sea level. Geophys. J. Int. 220, 384–392.
Pico, T., McGee, D., Russell, J., Mitrovica, J.X., 2020. Recent constraints on MIS 3 sea level support role of continental shelf exposure as a control on indo-pacific hydroclimate. Paleoceanogr. Paleoclimatol. 35, e2020PA003998 https://doi.org/10.1029/2020PA003998.
Pico, T., Birch, L., Weisenberg, J., Mitrovica, J.X., 2018. Refining the Laurentide Ice Sheet at Marine Isotope Stage 3: a data-based approach combining glacial isostatic simulations with a dynamic ice model. Quat. Sci. Rev. 195, 171–179.
Pico, T., Creveling, J.R., Mitrovica, J.X., 2017. sea-Level records from the U.S. Mid-atlantic constrain Laurentide ice sheet extent during marine isotope stage 3. Nat. Commun. 8, 1–6. https://doi.org/10.1038/ncomms15612.
Pico, T., Mitrovica, J.X., Ferrier, K.L., Braun, J., 2016. Global ice volume during MIS 3 inferred from a sea-level analysis of sedimentary core records in the Yellow River Delta. Quat. Sci. Rev. 152, 72–79.
Pirazzoli, P.A., 2005. A review of possible eustatic, isostatic and tectonic contributions in eight late-Holocene relative sea-level histories from the Mediterranean area. Quaternary Science Reviews 24, 1989–2001.
Pirazzoli, P.A., Montaggioni, L.F., Salvat, B., Faure, G., 1988. Late Holocene sea level indicators from twelve atolls in the central and eastern Tuamotus (Pacific Ocean). Coral Reefs 7, 57–68.
Robles, E.C., 2013. Estimates of Quaternary Philippine coastlines, land bridges, submerged river systems and migration routes: a GRASS GIS approach. Hukay 18.
Ryan, W.B., Carbotte, S.M., Coplan, J.O., O'Hara, S., Melkonian, A., Arko, R., Weissel, R. A., Ferrini, V., Goodwillie, A., Nitsche, F., 2009. Global multi-resolution topography synthesis. G-cubed 10.
Shipton, C., O'Connor, S., Jankowski, N., O'Connor-Veth, J., Maloney, T., Kealy, S., Boulanger, C., 2019. A new 44,000-year sequence from Asitau Kuru (Jerimalai), Timor-Leste, indicates long-term continuity in human behaviour. Archaeol. Anthropol. Sci. 11, 5717–5741.
Simms, A.R., Lisiecki, L., Gebbie, G., Whitehouse, P.L., Clark, J.F., 2019. Balancing the last glacial maximum (LGM) sea-level budget. Quat. Sci. Rev. 205, 143–153.
Spada, G., Galassi, G., 2017. Extent and dynamic evolution of the lost land aquaterra since the Last Glacial Maximum. Compt. Rendus Geosci. 349, 151–158.
Sturt, F., Garrow, D., Bradley, S., 2013. New models of north west European Holocene palaeogeography and inundation. J. Archaeol. Sci. 40, 3963–3976.
Tsuji, L.J.S., Daradich, A., Gomez, N., Hay, Mitrovica, J.X., 2016. sea level change in the western James Bay region of Subarctic Ontario. Emergent land and implications for Treaty No 9 (69), 99–107.
Turcotte, D., Schubert, G., 2014. Geodynamics, third ed. Cambridge University Press, Cambridge. https://doi.org/10.1017/CBO9780511843877.
Waelbroeck, C., Labeyrie, L., Michel, E., Duplessy, J.C., McManus, J.F., Lambeck, K., Balbon, E., Labracherie, M., 2002. Sea-level and deep water temperature changes derived from benthic foraminifera isotopic records. Quat. Sci. Rev. 21, 295–305.
Ward, I., Larcombe, P., Lillie, M., 2006. The dating of Doggerland–post-glacial geochronology of the southern North Sea. Environ. Archaeol. 11, 207–218.
Weninger, B., Schulting, R., Bradtmöller, M., Clare, L., Collard, M., Edinborough, K., Hilpert, J., Jöris, O., Niekus, M., Rohling, E.J., 2008. The catastrophic final flooding of Doggerland by the Storegga Slide tsunami. Documenta Praehistorica 35, 1–24.